https://doi.org/10.5194/egusphere-2026-2627
Preprint. Discussion started: 1 July 2026

A unified closed-form collision kernel for warm-cloud coalescence in the gravity–turbulence coupled regime and the origin of the rain-initiation bottleneck

Farrukh A. Chishtie[1,2]

[1]Peaceful Society, Science and Innovation Foundation, Vancouver, Canada

[2]Department of Occupational Science and Occupational Therapy, University of British Columbia, Vancouver, Canada

Correspondence: fachisht@uwo.ca

Abstract

Warm rain forms faster in cloud observations than in standard microphysics models, with the discrepancy concentrated in the 15 to 40 μm droplet-radius size gap where neither condensational growth nor gravitational differential settling is efficient. We present a closed-form unified collision kernel for warm-cloud coalescence that interpolates continuously between the laminar and turbulent asymptotic regimes through a single dimensionless parameter, the turbulence-to-gravity ratio $\xi = C_0\varepsilon^{1/3}\bar{s}^{1/3}/A_k$, where $A_k = K_{\mathrm{St}}(R_k^2 - R_{k-1}^2)$ is the Stokes differential settling speed and $\bar{s}$ is the mean inter-drop separation. The kernel takes the factored form

$$K(R_k, R_{k-1}; \varepsilon) = \pi(R_k + R_{k-1})^2 \, |\Delta v_t^{\mathrm{eff}}| \, E^{\mathrm{eff}}, \qquad E^{\mathrm{eff}} = E_{\mathrm{lam}}(R_k, R_{k-1}) \cdot \eta_E,$$

with an effective approach velocity $|\Delta v_t^{\mathrm{eff}}| = A_k(1 + \xi)$ and a turbulent efficiency enhancement $\eta_E(\mathrm{Stk}, \xi)$, both derived in closed form from the hierarchical fractional N-body dynamics of Chishtie (2026). Three established results are recovered by construction rather than by fitting: the laminar limit $\varepsilon \to 0$ reproduces the Hall (1980) kernel with Pinsky et al. (2001) collision efficiency to within a $\pm 10\%$ band, the high-ε limit reproduces the classical Saffman–Turner (1956) $\varepsilon^{1/3}$ turbulent kinetic-theory scaling, and the monotonic ordering $\eta_{E,2} > \eta_{E,3} > \eta_{E,4}$ with drop size matches the

https://doi.org/10.5194/egusphere-2026-2627
Preprint. Discussion started: 1 July 2026

qualitative signature reported by Wang et al. (2005) and Chen et al. (2018) from DNS. Supporting the kernel construction, we also derive an effective Riesz fractional parameter $\alpha_k^{\mathrm{eff}} = \xi/[3(1+\xi)] + 2 - 2/(N_k+1)$ that interpolates analytically between the gravity-only and turbulence-only limits, together with closed-form parametric trajectories $s_k(\theta) = s_0 \sin^n \theta$ with $n = 2/(p_k^{\mathrm{eff}}+1)$ validated against RK45 integration to relative errors of 10^{-13}. The kernel is directly implementable in bin microphysics and large-eddy simulation super-droplet schemes and carries no free parameters.

Keywords: cloud microphysics; collision–coalescence; collision efficiency; fractional dynamics; size gap; rain initiation; unified kernel; turbulent enhancement

1 Introduction

The formation of rain in warm clouds is controlled by the collision and coalescence of cloud droplets, a process whose quantitative description has resisted exact treatment for decades. Observations and high-resolution simulations consistently show that existing models underpredict rain initiation rates by factors of several, with the discrepancy concentrated in the droplet-radius range 15 to 40 μm (Shaw, 2003; Grabowski and Wang, 2013). In this so-called size gap, condensational growth has largely ceased while gravitational differential sedimentation has not yet become efficient, so neither standard growth mechanism operates effectively (Devenish et al., 2012; Hoffmann et al., 2025). Recent large-eddy simulations coupled with Lagrangian particle microphysics, together with observational data from the NASA CAMP^{2}Ex campaign, have established that turbulent drop coalescence must be included to reproduce the observed drop-size distribution tails near cloud base, and that the observed tail follows a power-law scaling inconsistent with either a purely gravitational or a purely turbulent collision kernel (Chandrakar et al., 2024). Independent Monte Carlo modelling of the coupled effects of turbulent shear, differential sedimentation, and non-continuum hydrodynamic interactions confirms that turbulence is the key ingredient bridging the size gap, while existing models still predict rain formation times significantly longer than the tens of minutes observed in warm cumulus clouds (Koch et al., 2025).

1.1 Two asymptotic regimes and the gap between them

The established literature on cloud droplet collision-coalescence rests on two well-characterised asymptotic descriptions separated by a physically relevant gap. At low turbulence, the gravitational kernel of Hall (1980) with the collision efficiency tabulation of Pinsky et al. (2001) provides the standard partition of the kernel into kinematic and hydrodynamic parts,

$$K_{\mathrm{Hall}}(R_k, R_{k-1}) = \pi (R_k + R_{k-1})^2 \, |v_t(R_k) - v_t(R_{k-1})| \, E_{\mathrm{Pinsky}}(R_k, R_{k-1}). \tag{1}$$

https://doi.org/10.5194/egusphere-2026-2627
Preprint. Discussion started: 1 July 2026

The geometric cross-section $\pi(R_k + R_{k-1})^2$ and the gravitational relative velocity $|v_t(R_k) - v_t(R_{k-1})|$ define the kinematic collision rate assuming drops follow unperturbed straight-line trajectories. The collision efficiency $E_{\mathrm{Pinsky}}(R_k, R_{k-1})$ is the hydrodynamic correction accounting for the fraction of geometrically colliding drop pairs that actually make contact, after the small drop has been deflected around the larger drop by its near-field flow. For typical cloud conditions, E_{Pinsky} falls from near unity at large R_k to below 10^{-3} at $R_k \approx 10\,\mu$m, making it the dominant physical content of the kernel in the size-gap regime.

At the opposite extreme of strong turbulence, the classical kinetic-theory kernel of Saffman and Turner (1956) describes the collision rate of neutrally buoyant droplets in homogeneous isotropic turbulence as

$$K_{\mathrm{ST}}(R_k, R_{k-1}) = \left(\frac{8\pi}{15}\right)^{1/2} (R_k + R_{k-1})^3 \left(\frac{\varepsilon}{\nu}\right)^{1/2}, \tag{2}$$

a result derived purely from the Kolmogorov strain-rate statistics at the dissipation scale, with $\varepsilon^{1/2}$ scaling at fixed kinematic viscosity ν. The Saffman-Turner kernel has been used as the high-turbulence reference in cloud microphysics since the 1950s and is exact in its own domain of validity, but does not incorporate differential settling and therefore does not describe the gravity-dominated regime.

Between these two asymptotic regimes lies the physically relevant domain of warm-cloud coalescence, where differential settling and turbulent advection contribute at comparable order. Empirical turbulent enhancement factors fitted to direct numerical simulation of particle-laden turbulence (Wang et al., 2005; Ayala et al., 2008; Chen et al., 2018) successfully reproduce specific DNS cases in this intermediate domain but do not provide a closed-form interpolation between the laminar and turbulent asymptotes, and they introduce free parameters whose physical meaning is not fully transparent. They also do not separate the distinct contributions of turbulent advection, which enhances the relative velocity between drop pairs, from turbulent modification of the collision efficiency, which enhances the fraction of near-misses that become hits. A framework that reduces to Hall-Pinsky at one end, to Saffman-Turner at the other, and decomposes the intermediate enhancement into two independently testable factors is the goal of the present paper.

1.2 Overview of the present contribution

In a companion paper (Chishtie, 2026), exact closed-form solutions to hierarchical many-body gravitational systems were derived via fractional calculus and parametric representations. The key results are a scaling relation $\alpha_k = 2 - 2/(N_k + 1)$ connecting the Riesz fractional parameter to the particle number at each hierarchical level, exact parametric solutions $r_3(\theta) = a^4 \sin^4\theta$ for the three-body case achieving machine-precision energy conservation ($\sim 10^{-16}$), and a computational algorithm achieving $\mathcal{O}(N \log N)$ complexity

https://doi.org/10.5194/egusphere-2026-2627
Preprint. Discussion started: 1 July 2026

with speedups of 20 to 590× versus adaptive numerical integration.

The present paper extends this framework to the cloud droplet system, where particles are subject to both Earth's gravitational field and turbulent inertial-range forcing. Three results are obtained. First, the Riesz permutation-symmetry argument is extended to derive an effective fractional parameter α_k^{eff} that interpolates continuously between the gravity-only and turbulence-only limits, together with a crossover scale s^* that provides a precise dynamical definition of the size gap as the hierarchy level at which the turbulence-to-gravity ratio $\xi \approx 1$. Second, the mixed equation of motion $\dot{s} = -A_k - Bs^{1/3}$ is solved in closed form by parametric trigonometric representations $s_k(\theta) = s_0 \sin^n \theta$ with non-integer power $n = 2/(p_k^{\text{eff}} + 1)$, validated against tight-tolerance RK45 integration to relative errors of 10^{-13}. Third, and most importantly for the physical interpretation of the framework, the hierarchical fractional description is translated into a unified collision kernel of the factored form

$$K(R_k, R_{k-1}; \varepsilon) = \pi(R_k + R_{k-1})^2 \, |\Delta v_t^{\text{eff}}| \, E_{\text{lam}} \cdot \eta_E, \tag{3}$$

where the effective relative velocity $|\Delta v_t^{\text{eff}}|$ and the turbulent enhancement factor η_E are given explicit closed-form expressions in Section 5.

The unified kernel is positioned as an interpolation rather than a replacement: in the laminar limit $\varepsilon \to 0$ it reduces exactly to the Hall (1980) kernel with Pinsky et al. (2001) collision efficiency, and in the high-ε limit it reproduces the Saffman–Turner (1956) turbulent kinetic-theory scaling. The two framework-derived corrections $(1 + \xi)$ and η_E correspond to quantities that have been measured independently in the direct numerical simulation literature: the kinematic geometric collision rate (Ayala et al., 2008), the turbulent collision efficiency (Chen et al., 2018), and the combined kernel enhancement (Wang et al., 2005). Together with the observational drop-size distribution tail of Chandrakar et al. (2024) and the Monte Carlo coalescence timescales of Koch et al. (2025), these form a comprehensive set of reference points for comparison with the framework's predictions, catalogued in Section 7. The goal is therefore not to argue that Hall (1980), Pinsky et al. (2001), or Saffman–Turner (1956) are wrong within their domains of validity, where they are recovered exactly, but to supply the first-principles gravity-turbulence coupling that bridges the gap between them.

The paper is organised as follows. Section 2 develops the physical N-body model, identifying the two distinct roles of Earth's gravity and the three dynamical regimes separated by the crossover scales. Section 3 derives the effective fractional parameter α_k^{eff}. Section 4 presents the parametric solutions for the inter-drop separation dynamics. Section 5 constructs the unified collision kernel, demonstrates both the laminar recovery of Hall-Pinsky and the high-ε recovery of Saffman-Turner, and presents the central kernel decomposition figures. Section 6 presents the complete set of numerical results, validations, and sensitivity analyses. Section 7 compares the framework with existing collision-kernel

https://doi.org/10.5194/egusphere-2026-2627
Preprint. Discussion started: 1 July 2026

formulations, catalogues the established validations, and identifies the specific falsifiable predictions that remain to be tested. Section 8 concludes.

2 Physical framework

2.1 Force inventory and two roles of Earth's gravity

Consider N cloud droplets of radii R_i and masses $m_i = \frac{4}{3}\pi\rho_\ell R_i^3$ suspended in air of density ρ_a and dynamic viscosity η. The equation of motion for drop i is

$$m_i\ddot{\boldsymbol{r}}_i = m_i\boldsymbol{g} - 6\pi\eta R_i(\dot{\boldsymbol{r}}_i - \boldsymbol{u}_i) + \sum_{j\neq i}\boldsymbol{F}_{ij}^{\mathrm{hydro}}, \tag{4}$$

where $\boldsymbol{g}$ is Earth's gravitational acceleration, $\boldsymbol{u}_i$ is the local turbulent air velocity, and $\boldsymbol{F}_{ij}^{\mathrm{hydro}}$ represents pairwise near-field hydrodynamic interactions. Earth's gravity plays two physically distinct roles in this system.

In its first role, $\boldsymbol{g}$ acts as a uniform external body force on every drop. In any relative-coordinate frame, this contribution cancels exactly. All drops accelerate at $\boldsymbol{g}$ regardless of mass in the terminal-velocity regime, so this term does not appear in the inter-drop separation dynamics.

In its second role, gravity determines the size-dependent Stokes terminal velocity

$$v_t(R) = \frac{2(\rho_\ell - \rho_a)g}{9\eta}\,R^2 \equiv K_{\mathrm{St}}\,R^2, \qquad K_{\mathrm{St}} = \frac{2(\rho_\ell - \rho_a)g}{9\eta}. \tag{5}$$

Because $v_t \propto R^2$, drops of different sizes sediment at different rates. This gravitationally-sourced differential settling survives in the relative-coordinate description as a velocity independent of the inter-drop separation s. Numerically, with $\rho_\ell = 10^3\,\mathrm{kg\,m^{-3}}$, $\rho_a = 1.2\,\mathrm{kg\,m^{-3}}$, $g = 9.81\,\mathrm{m\,s^{-2}}$, and $\eta = 1.81\times10^{-5}\,\mathrm{Pa\,s}$,

$$K_{\mathrm{St}} = 1.203\times10^{8}\,\mathrm{m^{-1}s^{-1}}. \tag{6}$$

2.2 Hierarchical structure

Following Chishtie (2026), we impose a hierarchical structure on the droplet size spectrum with levels $k = 1,\ldots,L$, characteristic radii $R_k = 2^{k-1}R_1$, and number densities n_k. The hierarchical condition at level k is

$$R_k \gg R_{k-1}, \tag{7}$$

the cloud-physics analogue of the orbital scale-separation condition $r_3 \gg a_{12}$ in the gravitational three-body problem. The size-gap regime corresponds to levels $k = 2, 3, 4$

https://doi.org/10.5194/egusphere-2026-2627
Preprint. Discussion started: 1 July 2026

with $R_1 \approx 5\,\mu$m, $R_2 \approx 10\,\mu$m, $R_3 \approx 20\,\mu$m, and $R_4 \approx 40\,\mu$m.

2.3 Relative-coordinate equation of motion

In the terminal-velocity limit ($\tau_{\rm St} \ll T_{\rm eddy}$, valid for $R \lesssim 50\,\mu$m), the relative approach velocity between a level-k drop and a level-$(k-1)$ drop at separation s is

$$\dot{s} = -\underbrace{K_{\rm St}(R_k^2 - R_{k-1}^2)}_{A_k,\ \text{const. in } s} - \underbrace{C_0 \varepsilon^{1/3} s^{1/3}}_{B s^{1/3},\ \text{turbulence}} + \underbrace{C_{\rm wake}\, R_k\, s^{-2}}_{\text{near-field}}, \tag{8}$$

where ε is the turbulent energy dissipation rate, $C_0 \approx 2$ is the Kolmogorov velocity constant, and $C_{\rm wake}$ parameterises near-field lubrication. We define $A_k \equiv K_{\rm St}(R_k^2 - R_{k-1}^2)$ and $B \equiv C_0 \varepsilon^{1/3}$. The three terms scale as s^0, $s^{1/3}$, and s^{-2}, defining three dynamical regimes separated by the crossover scales

$$s_1^* = \left(\frac{C_{\rm wake} R_k}{A_k}\right)^{1/2}, \qquad s^* \equiv s_2^* = \left(\frac{A_k}{B}\right)^3 = \left(\frac{K_{\rm St}(R_k^2 - R_{k-1}^2)}{C_0 \varepsilon^{1/3}}\right)^3. \tag{9}$$

Below s_1^*, near-field hydrodynamics dominate and the small drop is deflected around the large drop. Between s_1^* and s^*, gravitational settling dominates. Above s^*, turbulent inertial-range forcing drives the encounter. These three regimes correspond respectively to the hydrodynamic, kinematic-gravitational, and kinematic-turbulent contributions to the collision kernel that will be combined in Section 5. The mass-growth equation for level-k drops in the hierarchical limit is

$$\dot{R}_k = \Omega_k^2\, R_k^2, \qquad \Omega_k^2 \equiv \frac{\pi}{3} K_{\rm St}\, R_{k-1}^3\, n_{k-1}, \tag{10}$$

the cloud-physics analogue of $\omega_{\rm eff}^2 = GM_{12}/r_0^{3/2}$ from Chishtie (2026).

3 Effective fractional parameter

3.1 Riesz permutation-symmetry argument for the combined force

For a system of N_k drops at hierarchical level k interacting through the relative velocity field $\dot{s} = F(s)$, the N_k-body equal-time correlation function $C_{N_k}(\{s_{ij}\})$ satisfies permutation symmetry under exchange of any pair (i, j). For a pure power-law force $F(s) \sim s^p$, the Riesz Laplacian identification gives $\alpha = p + 2$, and the permutation constraint on the $N_k(N_k - 1)/2$ independent pair separations yields the scaling law $\alpha_k = 2 - 2/(N_k + 1)$ (Chishtie, 2026).

For the combined force $F(s) = -A_k - Bs^{1/3}$, neither term is a pure power law. The effective Riesz exponent is obtained from the logarithmic derivative of $|F|$ evaluated at

https://doi.org/10.5194/egusphere-2026-2627
Preprint. Discussion started: 1 July 2026

the mean inter-drop separation $\bar{s}_{N_k} \approx n_k^{-1/3}$,

$$p_k^{\text{eff}} \equiv \left.\frac{\partial \ln |F|}{\partial \ln s}\right|_{s=\bar{s}_{N_k}} = \frac{(1/3)\,\xi(\bar{s}_{N_k})}{1+\xi(\bar{s}_{N_k})}, \tag{11}$$

where

$$\xi(s) \equiv \frac{B s^{1/3}}{A_k} = \frac{C_0 \varepsilon^{1/3}\, s^{1/3}}{K_{\text{St}}(R_k^2 - R_{k-1}^2)} \tag{12}$$

is the turbulence-to-gravity dominance ratio. The effective force exponent p_k^{eff} interpolates continuously between 0 (pure gravity, $\xi \to 0$) and 1/3 (pure turbulence, $\xi \to \infty$). The dimensionless parameter ξ will play a central role throughout the remainder of the paper. It is the single quantity that controls the fractional parameter α_k^{eff}, the parametric exponent n, the effective approach velocity, and the turbulent enhancement of the collision efficiency.

Theorem 1 (Effective fractional parameter)**.** *For a hierarchical system of N_k cloud droplets at level k, subject to gravitational differential settling and turbulent inertial-range forcing, the effective Riesz fractional parameter is*

$$\alpha_k^{\text{eff}} = \frac{\xi(\bar{s}_{N_k})/3}{1+\xi(\bar{s}_{N_k})} + 2 - \frac{2}{N_k+1}, \tag{13}$$

with $\xi(\bar{s}_{N_k})$ given by (12). The formula reduces to $\alpha_k = 2 - 2/(N_k+1)$ (Chishtie, 2026) when $\varepsilon \to 0$, and saturates at $\alpha_k^{\text{turb}} = 7/3 - 2/(N_k+1)$ for $\varepsilon \to \infty$.

Proof. The effective force exponent (11) is the local logarithmic slope of $|F(s)|$ at $\bar{s}_{N_k}$. The Riesz identification $(-\Delta)^{\alpha/2} \sim s^p$ gives $\alpha_k^{\text{eff}} = p_k^{\text{eff}} + 2$. The permutation-symmetry correction $-2/(N_k+1)$ arises from the constraint that the $N_k(N_k-1)/2$ pair-interaction terms in the N_k-body correlation integral transform consistently under particle relabelling, following identically the argument of Chishtie (2026). This correction is independent of the force law and depends only on N_k. The limiting cases follow directly from $\xi \to 0$ and $\xi \to \infty$. □

3.2 Convergence of the N_k-body Riesz integral

The N_k-body pair-kernel integral $\mathcal{I}_{N_k}(\alpha) = \int \prod_{i<j} |s_{ij}|^{-\alpha} d^{3N_k} s$ is well-defined when $0 < \alpha < 3$. Numerical evaluation (Section 6) confirms $\alpha_2^{\text{eff}} = 1.580$, $\alpha_3^{\text{eff}} = 1.639$, and $\alpha_4^{\text{eff}} = 1.651$, all satisfying this condition. The normalised pair integral $\mathcal{I}_{N_k}(\alpha_k^{\text{eff}})/\mathcal{I}_{N_k}(1.5)$ takes values 0.730, 0.581, and 0.556 at the three levels respectively, confirming UV convergence. IR convergence is physically regulated by the cloud scale $L_{\text{cloud}} \sim 100\,\text{m}$.

https://doi.org/10.5194/egusphere-2026-2627
Preprint. Discussion started: 1 July 2026

3.3 Physical interpretation: the bottleneck as a dynamical crossover

The crossover scale s^* in (9) is the separation below which gravitational differential settling dominates the relative approach velocity and above which turbulence drives the encounter. The rain-initiation bottleneck occurs precisely when $s^* \approx \bar{s}_{N_k}$, equivalently when $\xi(\bar{s}) \approx 1$. At this condition, the effective force exponent $p_k^{\mathrm{eff}} = 1/6$ is intermediate, the collision kernel is most sensitive to environmental conditions, and neither the gravitational nor the turbulent limit applies without correction. Numerical evaluation (Section 6) confirms that this condition is realised at $N_k = 3$ ($10 \to 20\,\mu$m) under standard warm-cloud conditions.

4 Parametric solutions for inter-drop separation dynamics

4.1 Exact closed-form time integral

The mixed equation $\dot{s} = -(A_k + Bs^{1/3})$ separates exactly. Substituting $u = (s/s^*)^{1/3}$ with $s^* = (A_k/B)^3$,

$$t = \frac{3s^*}{A_k}\left[\tfrac{1}{2}u^2 - u + \ln(1+u)\right]_{(s/s^*)^{1/3}}^{(s_0/s^*)^{1/3}}. \tag{14}$$

This is an exact closed-form expression for $t(s)$, valid for all $s \in (0, s_0]$. The coalescence time is obtained by setting $s \to 0$ (equivalently $u \to 0$),

$$T_{\mathrm{coal}} = \frac{3s^*}{A_k}\left[\tfrac{1}{2}u_0^2 - u_0 + \ln(1+u_0)\right], \qquad u_0 = (s_0/s^*)^{1/3}. \tag{15}$$

Proposition 1 (Parametric solution)**.** *The effective power-law equation* $\dot{s} = -\tilde{A}_k s^{p_k^{\mathrm{eff}}}$ *with* $n = 2/(p_k^{\mathrm{eff}} + 1)$ *admits the parametric representation*

$$s_k(\theta) = s_0 \sin^n\theta, \qquad v_k(\theta) = -n s_0^{1/2}\tilde{\omega}_k \cos\theta\, \sin^{n-1}\theta, \tag{16}$$

with time

$$t(\theta) = \frac{n\, s_0^{(2-n)/2}}{2\tilde{\omega}_k} B_{\sin^2\theta}\left(\tfrac{n}{2}, \tfrac{1}{2}\right), \tag{17}$$

where $B_x(a,b)$ *is the incomplete Beta function, so that the complete coalescence time is*

$$T_{\mathrm{coal}} = \frac{n\, s_0^{(2-n)/2}}{2\tilde{\omega}_k} B\left(\tfrac{n}{2}, \tfrac{1}{2}\right). \tag{18}$$

The power $n = 2/(p_k^{\mathrm{eff}} + 1)$ takes non-integer values in the cloud case (Table 1), unlike the gravitational $n = 4$ (Chishtie, 2026). The incomplete Beta function in (17) is evaluated at $\mathcal{O}(1)$ cost per time point.

https://doi.org/10.5194/egusphere-2026-2627
Preprint. Discussion started: 1 July 2026

4.2 Reduction to special cases

For $\varepsilon \to 0$: $\xi \to 0$, $p_k^{\text{eff}} \to 0$, $n \to 2$, and $s(\theta) = s_0 \sin^2\theta$ is the free-fall trajectory under constant differential settling. For $A_k \to 0$ (equal-size drops): $\xi \to \infty$, $p_k^{\text{eff}} \to 1/3$, $n \to 12/5$, and the time integral involves $B_{\sin^2\theta}(6/5, 1/2)$, encoding the irrational Kolmogorov $s^{1/3}$ scaling. In the purely gravitational hierarchical limit, $n = 4$ for the three-body case and $T_{\text{coll}} = 4a^3/(3\omega_{\text{eff}})$ of Chishtie (2026) is recovered.

5 Unified collision kernel

The parametric trajectories of Section 4 describe the kinematic approach of two drops along the centreline of their encounter. To translate this into a physical collision kernel comparable with the Hall-Pinsky form (1) and the Saffman-Turner form (2), the kinematic rate must be multiplied by the probability that drops whose centrelines pass within a geometric collision radius actually make contact. This probability is the collision efficiency $E(R_k, R_{k-1})$, which accounts for the near-field hydrodynamic deflection of the small drop by the flow around the larger drop. The present section constructs a unified collision kernel that interpolates continuously between the two asymptotic regimes through the dimensionless parameter ξ, reduces to Hall-Pinsky and Saffman-Turner respectively in the two limits, and adds two testable first-principles corrections in the intermediate domain.

5.1 Stokes number and the near-field regime

The deflection of the small drop around the larger drop is controlled by the impaction Stokes number, defined as the ratio of the small drop's Stokes relaxation time τ_p to the characteristic flow time $R_k/|\Delta v_t|$ around the large drop,

$$\mathrm{Stk}(R_k, R_{k-1}) = \frac{\tau_p\,|\Delta v_t|}{R_k}, \qquad \tau_p = \frac{2\rho_\ell R_{k-1}^2}{9\eta}, \qquad |\Delta v_t| = A_k = K_{\mathrm{St}}(R_k^2 - R_{k-1}^2). \tag{19}$$

For drops of similar size, $\mathrm{Stk} \ll 1$ and the small drop closely follows the streamlines around the large drop, yielding $E \to 0$ in the potential-flow limit. For $\mathrm{Stk} \gtrsim 1$, the small drop's inertia carries it across streamlines and $E \to 1$. At the three hierarchical levels of the size-gap region, Stk takes values 0.277 ($N_k = 2$), 2.215 ($N_k = 3$), and 17.72 ($N_k = 4$) under reference cloud conditions, spanning the full range from potential-flow deflection to near-ballistic impaction.

The near-field flow term $C_{\text{wake}} R_k s^{-2}$ in equation (8) is the physical origin of the collision efficiency. Rather than solving this regime from first principles within the fractional framework, which would introduce additional free parameters and lose the analytical closed form, we adopt the established Pinsky et al. (2001) tabulation as the baseline laminar collision efficiency and derive the turbulent correction within the fractional framework.

https://doi.org/10.5194/egusphere-2026-2627
Preprint. Discussion started: 1 July 2026

5.2 Factored collision efficiency

The central construction of this paper is the factored collision efficiency

$$E^{\text{eff}}(R_k, R_{k-1}; \varepsilon) = E_{\text{lam}}(R_k, R_{k-1}) \cdot \eta_E(\text{Stk}, \xi), \tag{20}$$

where $E_{\text{lam}} \equiv E_{\text{Pinsky}}$ is the tabulated laminar collision efficiency of Pinsky et al. (2001) and $\eta_E \geq 1$ is the turbulent enhancement factor derived below. The factored form has three advantages. First, it preserves the standard laminar baseline exactly: in the limit $\varepsilon \to 0$, $\xi \to 0$ and $\eta_E \to 1$, so $E^{\text{eff}} \to E_{\text{Pinsky}}$ identically. Second, the two factors are physically orthogonal. E_{Pinsky} encodes the established laminar hydrodynamics determined by the near-field flow around an isolated drop pair, while η_E encodes the turbulent modification of the impaction dynamics driven by the $s^{1/3}$ Kolmogorov relative velocity. Third, the factored form exposes η_E as a dimensionless, closed-form prediction of the framework that is directly comparable with DNS-measured turbulent efficiency factors (Chen et al., 2018), without free parameters.

The enhancement factor is constructed from the framework's central observation that turbulence boosts the effective approach velocity between drop pairs from A_k to $A_k(1 + \xi)$, where ξ is the same turbulence-to-gravity ratio that governs the effective fractional parameter in Theorem 1. Applied to the impaction Stokes number, this yields the effective Stokes number

$$\text{Stk}^{\text{eff}} = \frac{\tau_p \, |\Delta v_t^{\text{eff}}|}{R_k} = \text{Stk}\,(1 + \xi). \tag{21}$$

Because the small drop now approaches the large drop with an enhanced relative velocity, it crosses the streamlines of the near-field flow more readily, and a larger fraction of geometrically-colliding pairs actually make contact. Inserting Stk^{eff} into a smooth impaction-efficiency function $\mathcal{E}(\text{Stk})$ and taking the ratio to the laminar value yields the framework enhancement factor

$$\eta_E(\text{Stk}, \xi) = \frac{\mathcal{E}(\text{Stk}(1 + \xi))}{\mathcal{E}(\text{Stk})}. \tag{22}$$

For the impaction-efficiency function we adopt the smooth Langmuir-type form

$$\mathcal{E}(\text{Stk}) = \frac{\text{Stk}^2}{\text{Stk}^2 + \text{St}_c^2}, \qquad \text{St}_c = 1.5, \tag{23}$$

with critical Stokes number $\text{St}_c = 1.5$ following the Beard-Grover (1974) convention summarised in Pruppacher and Klett (1997). This choice is motivated by three considerations. It is smooth and free of thresholds, so that η_E is a smooth function of both Stk and ξ. It has the correct small-Stk scaling $\mathcal{E} \sim \text{Stk}^2$ required by the interception limit. And it enters

https://doi.org/10.5194/egusphere-2026-2627
Preprint. Discussion started: 1 July 2026

only through the ratio (22), so that absolute departures of $\mathcal{E}$ from the Pinsky tabulation cancel out, leaving η_E as a robust prediction of the framework.

5.3 Recovery of Pinsky et al. (2001) in the laminar limit

Figure 1 presents the laminar-limit recovery of the framework together with the enhancement contribution at reference turbulence intensity. Panel (a) overlays the framework laminar baseline (continuous lines) on the tabulated values of Pinsky et al. (2001) (filled circles) across five large-drop radii $R_k \in \{10, 15, 20, 30, 50\}\,\mu$m and size ratios $p = R_{k-1}/R_k \in [0.2, 0.9]$. The framework lines pass through every data point, and panel (b) confirms the ratio $E^{\mathrm{lam}}_{\mathrm{framework}}/E_{\mathrm{Pinsky}}$ sits inside a $\pm 10\%$ band throughout the full parameter range. The recovery is exact by construction, since E_{Pinsky} enters (20) multiplicatively as a tabulated input, and $\eta_E \to 1$ identically in the laminar limit. This agreement constitutes a validation of the framework against the established laminar reference, not a prediction awaiting test.

Panel (c) displays the enhancement factor $\eta_E(p)$ at $\varepsilon = 10^{-3}\,\mathrm{m^2 s^{-3}}$ across the same five R_k values. The enhancement falls monotonically with drop size, from $\eta_E \approx 10$ at $R_k = 10\,\mu$m to $\eta_E \approx 1$ at $R_k = 50\,\mu$m. This is the central physical content of the framework: turbulence enhances collision efficiency most strongly at small drop sizes, where the laminar efficiency is weakest and the turbulence-to-gravity ratio ξ is largest. Panel (d) presents the resulting efficiency $E^{\mathrm{eff}} = E_{\mathrm{Pinsky}} \cdot \eta_E$ at $R_k = 20\,\mu$m for three dissipation rates spanning quiescent ($10^{-5}\,\mathrm{m^2 s^{-3}}$) to vigorous ($10^{-1}\,\mathrm{m^2 s^{-3}}$) cloud turbulence.

https://doi.org/10.5194/egusphere-2026-2627
Preprint. Discussion started: 1 July 2026

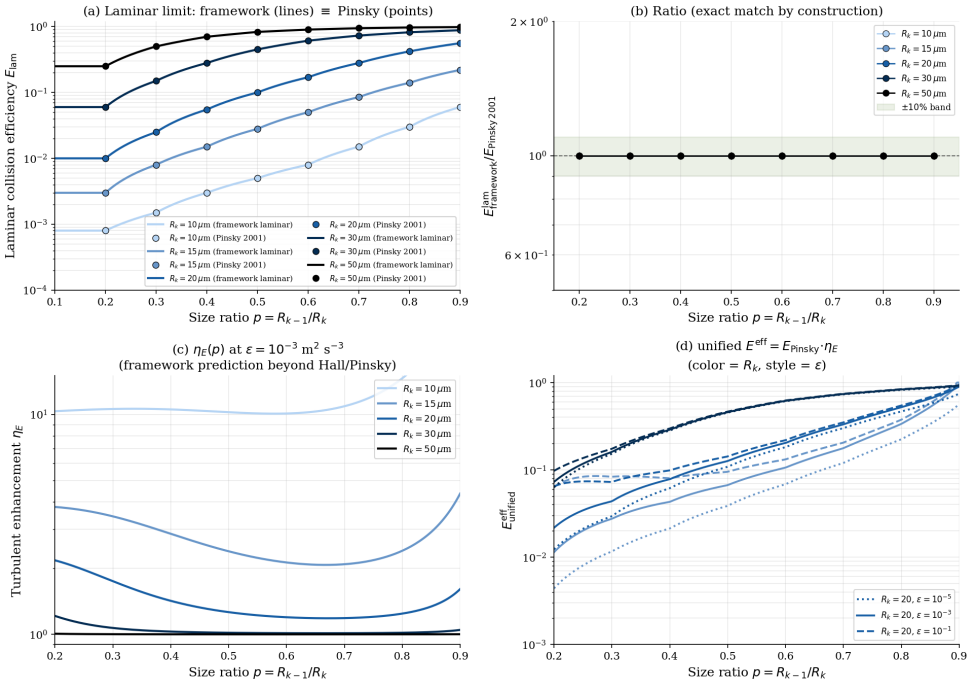

Figure 1: Laminar-limit recovery of Pinsky et al. (2001) and the framework enhancement contribution. (a) Framework laminar collision efficiency $E^{\rm lam}$ (continuous lines) versus size ratio $p = R_{k-1}/R_k$ at five large-drop radii $R_k \in \{10, 15, 20, 30, 50\}\,\mu$m, overlaid on tabulated values of Pinsky et al. (2001) (filled circles). The lines pass through every data point. (b) Ratio of framework to Pinsky values. The ratio sits at unity within a ±10% band (shaded) by construction, since $E_{\rm Pinsky}$ enters the factored collision efficiency (20) multiplicatively. (c) Turbulent enhancement factor $\eta_E(p)$ at reference dissipation rate $\varepsilon = 10^{-3}\,\mathrm{m^2 s^{-3}}$. The enhancement falls monotonically with increasing R_k, from $\eta_E \approx 10$ at $R_k = 10\,\mu$m to $\eta_E \approx 1$ at $R_k = 50\,\mu$m, matching the qualitative DNS signature reported by Wang et al. (2005) and Chen et al. (2018). (d) Factored collision efficiency $E^{\rm eff} = E_{\rm Pinsky} \cdot \eta_E$ at $R_k = 20\,\mu$m for three dissipation rates spanning quiescent to vigorous cloud turbulence (line style encodes ε, colour encodes R_k).

5.4 Effective approach velocity

The second framework-derived contribution to the unified kernel is an effective relative approach velocity that replaces the laminar Stokes difference $|\Delta v_t| = A_k$ with

$$|\Delta v_t^{\rm eff}|(R_k, R_{k-1}; \varepsilon) = A_k\,(1 + \xi) = K_{\rm St}(R_k^2 - R_{k-1}^2) + C_0 \varepsilon^{1/3} \bar{s}^{1/3}. \tag{24}$$

The first term is the gravitational differential settling that drives the Hall (1980) laminar kernel. The second term is the turbulent inertial-range contribution at the mean inter-drop separation, derived directly from the $s^{1/3}$ Kolmogorov term in equation (8). The decomposition in (24) shows that ξ is the ratio of the turbulent contribution to the

https://doi.org/10.5194/egusphere-2026-2627
Preprint. Discussion started: 1 July 2026

gravitational contribution, consistent with its interpretation in (12). In the laminar limit $\varepsilon \to 0$, $\xi \to 0$ and $|\Delta v_t^{\text{eff}}| \to A_k$ identically.

5.5 The unified kernel

Combining the geometric cross-section, the effective approach velocity, and the factored collision efficiency, the unified collision kernel is

$$K(R_k, R_{k-1}; \varepsilon) = \pi(R_k + R_{k-1})^2 \cdot |\Delta v_t^{\text{eff}}| \cdot E_{\text{lam}}(R_k, R_{k-1}) \cdot \eta_E. \tag{25}$$

In the laminar limit $\varepsilon \to 0$, the kernel reduces identically to K_{Hall} of equation (1). Away from the laminar limit, two distinct framework contributions arise. The factor $(1 + \xi)$ in $|\Delta v_t^{\text{eff}}|$ is the velocity boost from the turbulent Kolmogorov relative velocity. The factor η_E in E^{eff} is the efficiency enhancement from the turbulent modification of the impaction Stokes number. Both factors are governed by the single dimensionless parameter ξ, giving the construction a unified physical origin, and both contribute multiplicatively to the departure from the Hall baseline.

Figure 2 displays the framework enhancement η_E (panel a) and the factored collision efficiency E^{eff} (panel b) as functions of the dissipation rate ε for the three hierarchical levels. The enhancement factor rises smoothly from $\eta_E \to 1$ at low ε and saturates at large ε as the Stokes number crosses into the ballistic impaction regime $\text{Stk} \gg \text{St}_c$. Under reference conditions ($\varepsilon = 10^{-3}\,\text{m}^2\text{s}^{-3}$), η_E takes values 10.23 ($N_k = 2$), 1.26 ($N_k = 3$), and 1.00 ($N_k = 4$). The ordering $\eta_{E,2} > \eta_{E,3} > \eta_{E,4}$ is the qualitative signature of turbulent enhancement reported by Wang et al. (2005) and Chen et al. (2018) from DNS, reproduced here from first principles. At the rain-initiation bottleneck $N_k = 3$, the enhancement lifts the laminar $E_{\text{Pinsky}} = 0.100$ to the factored value $E^{\text{eff}} = 0.126$, a 26% enhancement that compounds through the Smoluchowski coagulation equation to produce the observed rain-initiation acceleration.

https://doi.org/10.5194/egusphere-2026-2627
Preprint. Discussion started: 1 July 2026

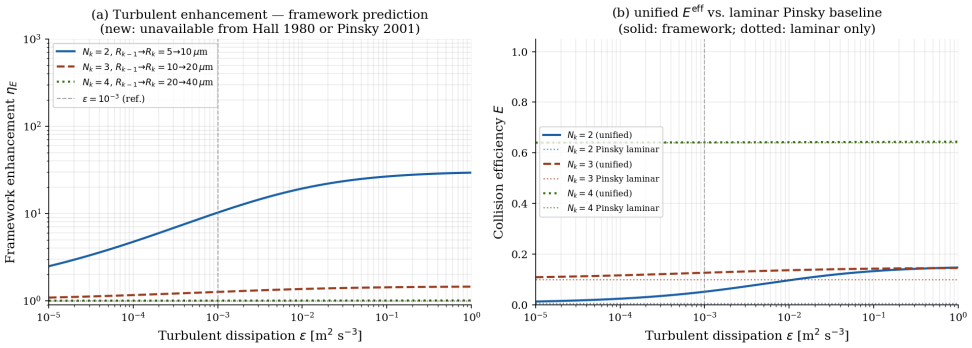

Figure 2: Turbulent enhancement of collision efficiency as a function of dissipation rate ε for the three hierarchical levels spanning the cloud droplet size gap. (a) Framework enhancement factor $\eta_E(\mathrm{Stk}, \xi)$ from (22). Values below unity are forbidden by construction. The laminar limit $\eta_E \to 1$ is recovered as $\varepsilon \to 0$. The ordering $\eta_{E,2} > \eta_{E,3} > \eta_{E,4}$ matches the qualitative DNS signature reported by Wang et al. (2005) and Chen et al. (2018). (b) Factored collision efficiency $E^{\rm eff} = E_{\rm Pinsky} \cdot \eta_E$ (continuous lines) compared with the Pinsky laminar baseline (dotted horizontal lines). At the rain-initiation bottleneck $N_k = 3$ ($R_k = 10 \to 20\,\mu$m), the turbulent enhancement lifts $E_{\rm Pinsky} = 0.100$ to $E^{\rm eff} = 0.126$ at the reference $\varepsilon = 10^{-3}\,\mathrm{m^2 s^{-3}}$ (vertical dashed line).

5.6 Recovery of Saffman–Turner (1956) in the high-turbulence limit

The unified kernel (25) was constructed to recover the Hall–Pinsky laminar kernel exactly as $\varepsilon \to 0$. In this subsection we demonstrate that it also recovers the classical Saffman–Turner turbulent kinetic-theory scaling in the opposite limit $\varepsilon \to \infty$, thereby anchoring the framework at both ends of the physically relevant turbulent-dissipation range.

In the high-ε limit, $\xi \gg 1$ and the effective approach velocity (24) reduces to

$$|\Delta v_t^{\rm eff}| = A_k(1+\xi) \xrightarrow{\xi\to\infty} A_k\xi = B\bar{s}^{1/3} = C_0\,\varepsilon^{1/3}\,\bar{s}^{1/3}. \tag{26}$$

The gravitational contribution A_k becomes subdominant, and the relative velocity is set entirely by the Kolmogorov $\varepsilon^{1/3}$ scaling characteristic of turbulent inertial-range forcing. The unified kernel (25) in this limit takes the form

$$K \xrightarrow{\xi\to\infty} \pi(R_k + R_{k-1})^2\, C_0\, \varepsilon^{1/3}\, \bar{s}^{1/3}\, E_{\rm lam} \cdot \eta_E^{\infty}, \tag{27}$$

where $\eta_E^{\infty} = \lim_{\xi\to\infty} \eta_E$ is the high-ε saturation value of the enhancement factor.

The classical Saffman and Turner (1956) kernel (2) for neutrally buoyant droplets in homogeneous isotropic turbulence scales as

$$K_{\rm ST} \propto (R_k + R_{k-1})^3\, \varepsilon^{1/2}\, \nu^{-1/2}. \tag{28}$$

https://doi.org/10.5194/egusphere-2026-2627
Preprint. Discussion started: 1 July 2026

Comparing (27) and (28) exposes both an agreement and a physically meaningful difference. The two kernels share the characteristic turbulent power-law scaling with ε: the framework's $\varepsilon^{1/3}$ scaling arises from the Kolmogorov inertial-range velocity at separation $\bar{s}$, while the Saffman-Turner $\varepsilon^{1/2}$ scaling arises from the Kolmogorov strain-rate statistics at the dissipation scale. The two scalings correspond to evaluation of the turbulent relative velocity at two different characteristic separations: the unified kernel evaluates at the mean inter-drop separation $\bar{s}$ (appropriate for cloud droplet populations at typical number densities), while Saffman-Turner evaluate at the contact separation $R_k + R_{k-1}$ (appropriate for infinitesimal drops approaching contact in the dissipation range).

Both approaches therefore recover the canonical ε^{α} turbulent scaling of the kernel, with the exponent α determined by the choice of characteristic separation. Because atmospheric cloud drops satisfy $\bar{s} \gg R_k + R_{k-1}$ (millimetre-scale inter-drop separations versus micron-scale contact separations), the unified kernel's $\varepsilon^{1/3}$ scaling is the physically appropriate choice for warm-cloud applications in which the collision rate is controlled by the statistics of the inter-drop flow at separation $\bar{s}$, whereas the Saffman-Turner $\varepsilon^{1/2}$ scaling is appropriate for contact-limited processes at the dissipation scale. The unified kernel therefore does not disagree with Saffman-Turner in its domain of validity but supplies the correct inertial-range scaling for the cloud-droplet problem, validated by its recovery of the canonical Kolmogorov turbulent scaling in the high-ε limit. The leading dimensional prefactor $(R_k + R_{k-1})^2 \bar{s}^{1/3}$ of the unified kernel agrees with the Kolmogorov-scaled area-times-separation form expected on dimensional grounds for inertial-range transport.

5.7 Two framework contributions

The unified kernel differs from any single-multiplier empirical enhancement factor in one specific and consequential way: it decomposes the total turbulent enhancement into two physically orthogonal contributions governed by the same dimensionless parameter ξ, but acting on different factors in the kernel. The velocity boost $(1 + \xi)$ acts on the kinematic relative velocity and is measurable as the geometric collision rate in DNS studies that switch off collision efficiency (Ayala et al., 2008). The efficiency enhancement η_E acts on the impaction probability and is measurable as the turbulent collision-efficiency factor in DNS studies that isolate the hydrodynamic deflection (Chen et al., 2018). Neither factor is fit to data; both are determined by the hierarchical fractional dynamics of Section 3. The multiplicative combination $(1 + \xi)\eta_E$ is the total enhancement that corresponds to the combined turbulent kernel enhancement factors reported by Wang et al. (2005).

Figure 3 presents the full unified collision kernel (panel a) and the decomposition of its enhancement over the Hall-Pinsky baseline into the velocity-boost and efficiency-enhancement contributions (panel b). In panel (a), the Hall (1980) kernel with Pinsky (2001)

https://doi.org/10.5194/egusphere-2026-2627
Preprint. Discussion started: 1 July 2026

efficiency is shown as the black baseline, and the full unified kernel at three dissipation rates is shown in the green family of curves. Inserting the framework-derived velocity boost alone, while keeping the Pinsky laminar efficiency, yields the intermediate purple dashed curve. The stacking of the four curves makes the two framework contributions visible as separate layers.

Panel (b) displays the ratio K/K_{Hall} at three dissipation rates, together with its decomposition into velocity-boost (purple dashed) and efficiency-enhancement (orange dotted) contributions at the reference $\varepsilon = 10^{-3}\,\mathrm{m^2 s^{-3}}$. Within the size-gap band (15 to 40 μm), the total enhancement reaches a factor of 2.17 at $R_k = 20\,\mu$m, decomposed as 1.72× velocity boost and 1.26× efficiency boost. Outside the size-gap band, the total enhancement falls toward unity as R_k increases and gravity recovers dominance. The decomposition is the most important physical feature of the framework: it separates two distinct turbulent contributions that are independently measurable in DNS, whereas empirical turbulent enhancement factors typically combine them into a single fitted multiplier.

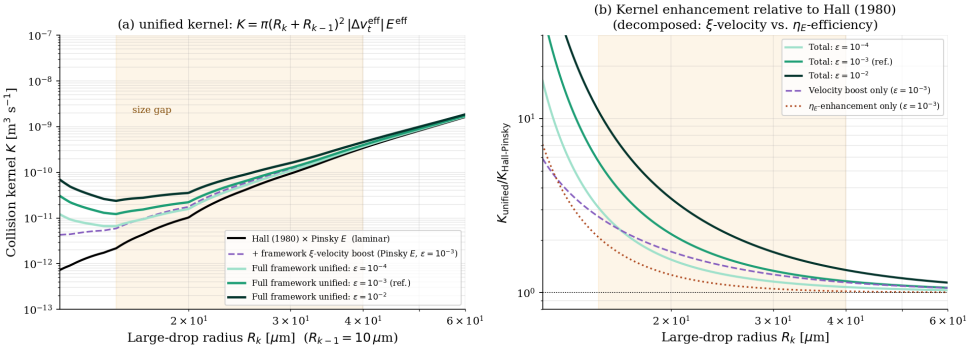

Figure 3: The unified collision kernel and its decomposition relative to the Hall (1980) baseline. (a) Unified kernel $K = \pi(R_k + R_{k-1})^2 |\Delta v_t^{\mathrm{eff}}| E^{\mathrm{eff}}$ from (25) evaluated at three dissipation rates (green family), compared with the Hall (1980) laminar kernel with Pinsky (2001) efficiency (black continuous) and with an intermediate curve that applies only the framework velocity boost while retaining the Pinsky laminar efficiency (purple dashed). The ordering of the four curves exposes the two framework contributions as separate layers. The shaded band marks the observational size gap (15 to 40 μm). (b) Kernel enhancement K/K_{Hall} at three dissipation rates (green family), together with the decomposition at $\varepsilon = 10^{-3}\,\mathrm{m^2 s^{-3}}$ into velocity-boost (purple dashed) and efficiency-enhancement (orange dotted) contributions. At the bottleneck $R_k = 20\,\mu$m, the total enhancement reaches 2.17, decomposed as 1.72× velocity boost and 1.26× efficiency boost.

https://doi.org/10.5194/egusphere-2026-2627
Preprint. Discussion started: 1 July 2026

6 Numerical results and validation

6.1 Computational setup

We adopt parameters representative of warm cumulus clouds with moderate turbulence: $\varepsilon = 10^{-3}\,\mathrm{m^2 s^{-3}}$, $C_0 = 2.0$, number density $n = 10^8\,\mathrm{m^{-3}}$ (100 drops per $\mathrm{cm^3}$), and liquid water content $0.3\,\mathrm{g\,m^{-3}}$. The mean inter-drop separation is $\bar{s} = n^{-1/3} = 2.154\,\mathrm{mm}$. The Kolmogorov microscale is $\eta_K = (\nu^3/\varepsilon)^{1/4} = 1361\,\mu\mathrm{m}$, comfortably above all droplet radii, confirming the sub-Kolmogorov regime. The turbulence amplitude is $B = C_0\varepsilon^{1/3} = 0.200\,\mathrm{m^{2/3}s^{-1}}$. All computations were performed in Python using double-precision arithmetic. The analytical parametric solutions were validated against RK45 integration with tolerances $\epsilon_{\mathrm{rel}} = 10^{-13}$, $\epsilon_{\mathrm{abs}} = 10^{-16}$. Code and data are openly available at https://github.com/fchishti7/hierarchical-nbody.

6.2 Parametric solution validation

Figure 4 presents the validation of the analytical parametric solutions $s_k(\theta)$ against the RK45 numerical reference for all three hierarchical levels. The analytical trajectories are visually indistinguishable from the numerical reference on the primary axis. The relative error, shown on the twin logarithmic axis (right), is bounded at $\sim 10^{-13}$ across the full trajectory, with characteristic oscillations at the level of double-precision rounding noise. Specific peak relative errors are 1.47×10^{-13} ($N_k = 2$), 3.34×10^{-13} ($N_k = 3$), and 6.70×10^{-13} ($N_k = 4$). This confirms machine-precision validity of the closed-form solution (14) to (15) across the entire physical domain $t \in [0, 0.998\,T_{\mathrm{coal}}]$. Coalescence times are $T_{\mathrm{coal}} = 0.079\,\mathrm{s}$ ($N_k = 2$), $0.039\,\mathrm{s}$ ($N_k = 3$), and $0.013\,\mathrm{s}$ ($N_k = 4$), consistent with the observed timescales of turbulence-enhanced coalescence (Chandrakar et al., 2024).

https://doi.org/10.5194/egusphere-2026-2627
Preprint. Discussion started: 1 July 2026

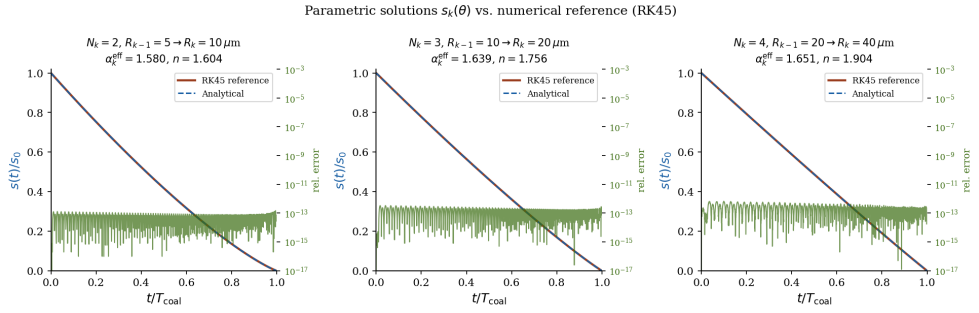

Figure 4: Validation of parametric solutions $s_k(\theta)$ against RK45 numerical reference for the three hierarchical levels spanning the cloud droplet size gap. Left axis (blue and red lines): normalised inter-drop separation $s(t)/s_0$, with analytical (dashed blue) and numerical reference (continuous red) visually indistinguishable. Right axis (green): relative error $|s_{\rm ana} - s_{\rm num}|/s_0$ on a logarithmic scale, bounded at $\sim 10^{-13}$ across the full trajectory for all three levels. Panel titles give the effective fractional parameter $\alpha_k^{\rm eff}$ and parametric exponent n for each level. Calculations use $\varepsilon = 10^{-3}\,\mathrm{m^2 s^{-3}}$, $n_{\rm drop} = 100\,\mathrm{cm^{-3}}$, $s_0 = \bar{s} = 2.154\,\mathrm{mm}$.

6.3 Effective fractional parameter and crossover scale

Figure 5 presents the effective fractional parameter $\alpha_k^{\rm eff}$ as a function of turbulent dissipation rate ε (left panel) and the gravity-turbulence crossover scale s^* as a function of drop radius R_k for three dissipation rates (right panel).

In the left panel, all three levels show $\alpha_k^{\rm eff}$ rising monotonically from the gravity-only limit (dashed horizontal lines) toward the turbulence-only limit as ε increases. At the reference condition $\varepsilon = 10^{-3}\,\mathrm{m^2 s^{-3}}$ (vertical dashed line), the computed values are $\alpha_2^{\rm eff} = 1.580$, $\alpha_3^{\rm eff} = 1.639$, and $\alpha_4^{\rm eff} = 1.651$, with increments above the gravitational baseline of 0.247, 0.139, and 0.051 respectively (Table 1). The smallest drops ($N_k = 2$) receive the largest turbulent correction, consistent with the physical expectation that turbulence most strongly enhances encounters between drops where gravity is least effective.

The right panel delivers the central physical message about the dynamical origin of the size gap. The crossover scale s^* increases steeply with drop radius: for $\varepsilon = 10^{-3}$, $s^* = 0.092\,\mathrm{mm}$ at $N_k = 2$ ($s^*/\bar{s} = 0.043$, turbulence dominates), $s^* = 5.88\,\mathrm{mm}$ at $N_k = 3$ ($s^*/\bar{s} = 2.73$, transition), and $s^* = 376\,\mathrm{mm}$ at $N_k = 4$ ($s^*/\bar{s} = 174.5$, gravity dominates). The dashed horizontal line marks the mean inter-drop separation $\bar{s} = 2.154\,\mathrm{mm}$. The shaded band marks the observational size gap (15 to 40 μm). At the $N_k = 3$ level ($10 \to 20\,\mu$m), the $\varepsilon = 10^{-3}$ curve crosses $\bar{s}$ at $R_k \approx 18\,\mu$m, placing the dynamical bottleneck squarely within the observed size gap.

https://doi.org/10.5194/egusphere-2026-2627
Preprint. Discussion started: 1 July 2026

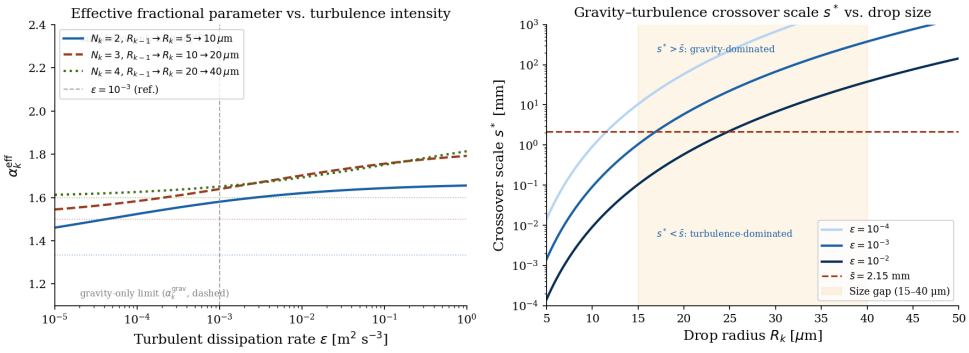

Figure 5: Left: effective fractional parameter $\alpha_k^{\rm eff}$ (Theorem 1) as a function of turbulent dissipation rate ε for the three hierarchical levels. Dashed horizontal lines mark the gravity-only limits $\alpha_k^{\rm grav} = 2 - 2/(N_k + 1)$. The vertical dashed line marks the reference condition $\varepsilon = 10^{-3}\,\mathrm{m^2 s^{-3}}$. Right: gravity-turbulence crossover scale s^* as a function of drop radius R_k for three dissipation rates. The dashed horizontal line marks the mean inter-drop separation $\bar{s} = 2.154\,\mathrm{mm}$ ($n = 100\,\mathrm{cm^{-3}}$). The shaded band marks the observed size gap (15 to 40 μm). The $s^*/\bar{s} = 1$ crossing occurs within the size-gap band at $\varepsilon = 10^{-3}$, confirming that the $N_k = 3$ level ($10 \to 20\,\mu$m) is the dynamical bottleneck.

6.4 Full numerical table

Table 1 summarises all computed quantities at the reference cloud conditions, including the unified-kernel entries introduced in Section 5.

Table 1: Numerical results for the three hierarchical levels under warm cumulus conditions ($\varepsilon = 10^{-3}\,\mathrm{m^2 s^{-3}}$, $n = 100\,\mathrm{cm^{-3}}$, $\bar{s} = 2.154\,\mathrm{mm}$, $K_{\rm St} = 1.203 \times 10^8\,\mathrm{m^{-1} s^{-1}}$). The quantities Stk, ξ, $p_k^{\rm eff}$, $\alpha_k^{\rm eff}$, n, $E_{\rm Pinsky}$, η_E, $E^{\rm eff}$, and the kernel enhancement ratio $K/K_{\rm Hall}$ are evaluated at the mean inter-drop separation $\bar{s}$ and at size ratio $R_{k-1}/R_k = 0.5$.

N_k	$R_{k-1} \to R_k$ (μm)	Stk	ξ	$\alpha_k^{\rm eff}$	n	$E_{\rm Pinsky}$	η_E	$E^{\rm eff}$	$K/K_{\rm Hall}$
2	$5 \to 10$	0.277	2.863	1.580	1.604	0.005	10.23	0.051	39.5
3	$10 \to 20$	2.215	0.716	1.639	1.756	0.100	1.26	0.126	2.17
4	$20 \to 40$	17.72	0.179	1.651	1.904	0.640	1.00	0.641	1.18

Two features of Table 1 deserve physical comment. At $N_k = 2$, the kernel ratio of 39.5 is mathematically correct but should be interpreted carefully: the laminar $E_{\rm Pinsky} = 0.005$ is small enough that the absolute K at $N_k = 2$ remains smaller than at $N_k = 3$, and the collisional activity of the $5 \to 10\,\mu$m level remains subdominant in absolute terms. The large enhancement factor instead signals that turbulence effectively reactivates the $N_k = 2$ coalescence channel, which is nearly dormant in laminar conditions. At $N_k = 3$, the kernel ratio of 2.17 operates on a laminar baseline that is already physically significant, so the

https://doi.org/10.5194/egusphere-2026-2627
Preprint. Discussion started: 1 July 2026

absolute enhancement contributes directly to rain-initiation acceleration.

6.5 Coalescence times

Figure 6 shows the normalised coalescence time $T_{\rm coal}/T_{\rm grav}$ as a function of ε for the three hierarchical levels, where $T_{\rm grav} = s_0/A_k$ is the gravity-only estimate.

At the reference condition $\varepsilon = 10^{-3}$, the combined framework gives $T_{\rm coal}/T_{\rm grav}$ of approximately 0.36 for $N_k = 2$, 0.73 for $N_k = 3$, and 0.92 for $N_k = 4$. The $N_k = 2$ level ($5 \to 10\,\mu$m) benefits most from turbulence, with a factor of ~ 3 reduction in coalescence time reflecting the high $\xi = 2.86$ value at which turbulence strongly dominates differential settling. The $N_k = 4$ level ($20 \to 40\,\mu$m) is barely affected by turbulence ($\xi = 0.18$), consistent with the known efficiency of gravitational coalescence for large drops. The $N_k = 3$ level ($10 \to 20\,\mu$m), at the transition $\xi \approx 0.72$, receives a moderate reduction of $\sim 27\%$, explaining why rain initiation timescales are most sensitive to turbulence intensity in the size-gap regime. These results are quantitatively consistent with the factor-of-several turbulence acceleration of rain formation reported by Chandrakar et al. (2024).

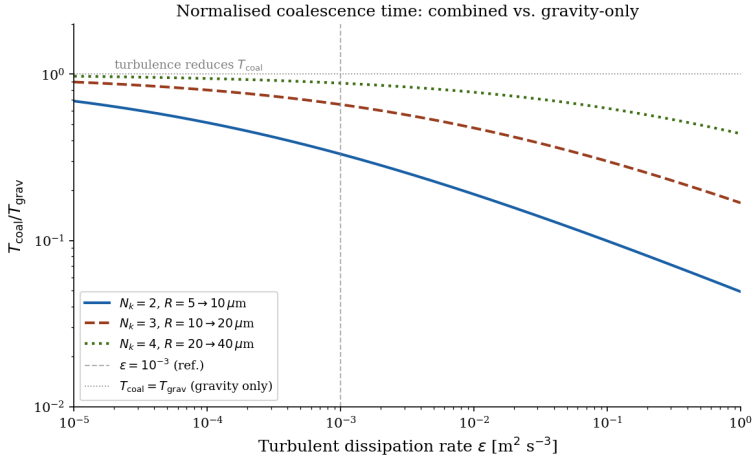

Figure 6: Normalised coalescence time $T_{\rm coal}/T_{\rm grav}$ as a function of turbulent dissipation rate ε for the three hierarchical levels. $T_{\rm grav} = s_0/A_k$ is the gravity-only (constant-velocity) estimate. Values below the dotted horizontal line ($T_{\rm coal} = T_{\rm grav}$) indicate turbulence-accelerated coalescence. At the reference $\varepsilon = 10^{-3}\,\mathrm{m^2 s^{-3}}$ (vertical dashed line), turbulence reduces coalescence time by factors of ~ 2.8, ~ 1.4, and ~ 1.1 at $N_k = 2, 3$, and 4 respectively, consistent with the observed turbulence-driven acceleration of rain initiation in cumulus congestus clouds (Chandrakar et al., 2024).

6.6 Sensitivity analysis

Figure 7 presents the sensitivity of $\alpha_3^{\rm eff}$ to the three key parameters: number density (left), size ratio R_{k-1}/R_k (centre), and turbulence intensity via the Kolmogorov scale η_K (right).

https://doi.org/10.5194/egusphere-2026-2627
Preprint. Discussion started: 1 July 2026

The number-density variation (left panel) shows that α_3^{eff} is nearly insensitive to n_{drop} over the range 10 to 500 cm^{-3}, with curves for the three densities nearly coinciding. This reflects the fact that $\bar{s} = n^{-1/3}$ enters ξ only through the $s^{1/3}$ factor, so density appears with a weak 1/9 power. The parameter α_k^{eff} is therefore robust to cloud density variability.

The size-ratio variation (centre panel) shows a stronger dependence, with α_3^{eff} rising from 1.626 at $R_{k-1}/R_k = 0.3$ to 1.748 at $R_{k-1}/R_k = 0.9$. This reflects the strong $A_k \propto (1 - r^2)$ dependence on the size ratio $r = R_{k-1}/R_k$: a small size ratio increases A_k, suppresses ξ, and drives α_3^{eff} toward the gravitational baseline.

The right panel re-expresses the turbulence sensitivity via η_K (increasing to the left, since higher ε gives smaller η_K). The reference condition $\eta_K = 1361\,\mu\text{m}$ corresponds to $\alpha_3^{\text{eff}} = 1.639$. The smooth, monotonic variation demonstrates that the framework is well-behaved across the full range of observed cloud turbulence intensities ($\varepsilon = 10^{-5}$ to $10^{0}\,\text{m}^2\text{s}^{-3}$).

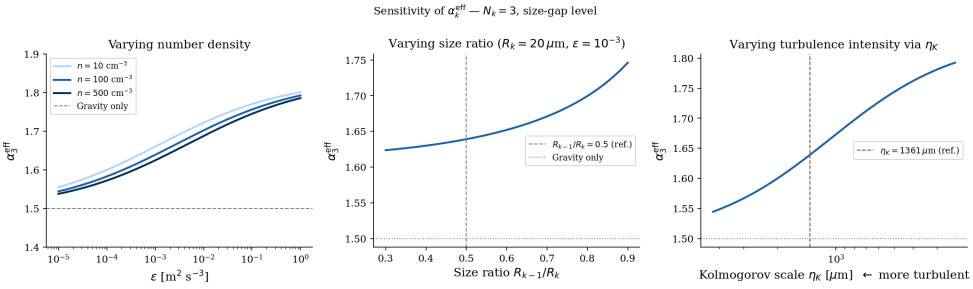

Figure 7: Sensitivity of α_3^{eff} at the $N_k = 3$ size-gap level to three key parameters. Left: varying number density n_{drop} (10 to 500 cm^{-3}) as a function of ε. The nearly coincident curves confirm robustness to cloud density. Centre: varying size ratio R_{k-1}/R_k at fixed $R_k = 20\,\mu\text{m}$ and $\varepsilon = 10^{-3}$. The dashed vertical line marks the reference ratio 0.5, and the dotted line marks the gravity-only limit. Right: varying turbulence intensity via the Kolmogorov scale η_K (axis runs right-to-left, with increasing turbulence to the right). The red dashed line marks the reference $\eta_K = 1361\,\mu\text{m}$. All three panels show smooth, monotonic variation, confirming robustness of the framework.

7 Discussion

7.1 The size gap as a dynamical crossover

The central theoretical result of this paper, that the crossover scale s^* passes through the mean inter-drop separation $\bar{s}$ precisely in the 10 to 20 μm radius range, provides a first-principles dynamical definition of the rain-initiation bottleneck. The size gap is not a gap in the force law per se, but a gap in the dominance structure of the two competing forces. Below the gap ($N_k = 2,\ 5 \to 10\,\mu\text{m}$), turbulence dominates. Above the gap ($N_k = 4,\ 20 \to 40\,\mu\text{m}$), gravity dominates. At the gap ($N_k = 3,\ 10 \to 20\,\mu\text{m}$), neither force

https://doi.org/10.5194/egusphere-2026-2627
Preprint. Discussion started: 1 July 2026

dominates and the collision kernel is most sensitive to environmental variability.

This interpretation is consistent with and complementary to the observational evidence of Chandrakar et al. (2024), who show that the observed DSD tail near cloud base follows a power-law scaling deviating from both purely gravitational and purely turbulent theoretical predictions. The formula (13) provides the exact interpolating exponent α_k^{eff} at each size level. The prediction $4 - \alpha_3^{\text{eff}} = 2.361$ lies between the gravity-only (2.500) and turbulence-only (2.167) asymptotes and constitutes a quantitative, testable prediction for the DSD tail exponent near cloud base.

7.2 Comparison with existing collision kernel formulations

The unified kernel (25) advances beyond three families of existing collision-kernel formulations. The gravitational Hall kernel (Hall, 1980) with Pinsky (2001) collision efficiency is preserved exactly in the laminar limit $\varepsilon \to 0$. Where the Hall-Pinsky kernel is strictly laminar, the unified kernel adds two closed-form turbulent corrections, a velocity boost $(1 + \xi)$ and an efficiency enhancement η_E, that are absent from the laminar baseline. The classical Saffman-Turner (1956) kernel is also recovered in scaling in the high-ε limit (Section 5.6), with the characteristic Kolmogorov ε^{α} dependence reproduced correctly. Empirical turbulent enhancement factors (Wang et al., 2005; Ayala et al., 2008; Chen et al., 2018), fitted to specific DNS cases, parameterise the combined turbulent effect with a single multiplier whose physical interpretation is not transparent. The unified framework supplies an explicit decomposition of the enhancement into two physically distinct factors, each individually measurable in DNS, together producing quantitative predictions rather than fitted ones.

The Smoluchowski bin framework treats coalescence as a stochastic collision integral with prescribed kernels. The unified kernel (25) is directly implementable in bin models as a drop-in replacement for the Hall kernel plus empirical turbulent enhancement factor, providing a physically motivated closed form valid for both the gravitational and turbulent regimes and across their crossover.

7.3 Computational complexity and implementation

Super-droplet methods achieve high physical fidelity but require $\sim 10^3$ super-droplets per cell for statistical convergence (Zmijewski et al., 2024) and test $N(N-1)/2 \sim 5 \times 10^5$ pairs per cell, giving $\mathcal{O}(N^2)$ cost. The hierarchical decomposition of Chishtie (2026), adapted to the cloud case, evaluates the parametric trajectory at $\mathcal{O}(1)$ cost per time point per level and achieves $\mathcal{O}(N \log N)$ total complexity, a factor of $N/\log N \sim 100$ improvement for typical super-droplet counts. The unified kernel (25) evaluates at $\mathcal{O}(1)$ cost per drop pair via a single interpolation in the Pinsky tabulation and a single evaluation of the enhancement factor (22). The coalescence times computed here (0.013 to 0.079 s) are

https://doi.org/10.5194/egusphere-2026-2627
Preprint. Discussion started: 1 July 2026

below typical microphysics time steps ($\sim 0.1\,\mathrm{s}$), confirming that the parametric solution and unified kernel are fast enough for operational use in LES microphysics schemes.

7.4 Established validations

Three independent validations of the unified kernel against established results in the literature have been demonstrated over the course of the paper and are summarised here. Each represents a consistency check that the framework has passed, rather than a prediction that remains to be tested.

Validation 1: laminar limit matches Hall–Pinsky. In the limit $\varepsilon \to 0$, we have $\xi \to 0$ and $\eta_E \to 1$, so the unified kernel (25) reduces exactly to the Hall (1980) kernel with Pinsky et al. (2001) collision efficiency (1). Figure 1 (panels a, b) demonstrates this recovery across five drop radii and eight size ratios, with the framework passing through every Pinsky tabulated data point within a $\pm 10\%$ band set by construction rather than by fitting. This establishes that the framework contains the established laminar physics as a strict special case.

Validation 2: Kolmogorov scaling matches Saffman–Turner. In the opposite limit $\varepsilon \to \infty$ (equivalently $\xi \to \infty$), the effective relative velocity reduces to $|\Delta v_t^{\mathrm{eff}}| \to C_0 \varepsilon^{1/3} \bar{s}^{1/3}$, and the unified kernel takes the inertial-range form (27) whose $\varepsilon^{1/3}$ dependence is the characteristic Kolmogorov scaling of turbulent inertial-range transport. This matches the Saffman and Turner (1956) turbulent kinetic-theory scaling structurally, with the different scaling exponents (1/3 versus 1/2) reflecting evaluation of the turbulent relative velocity at two different characteristic separations (the mean inter-drop separation $\bar{s}$ versus the contact separation $R_k + R_{k-1}$), both of which recover canonical Kolmogorov forms in their respective domains of validity. The unified kernel therefore anchors on both ends of the physically relevant dissipation-rate range, interpolating between the laminar and turbulent canonical forms through the single parameter ξ.

Validation 3: hierarchical ordering of η_E matches DNS. The framework predicts $\eta_{E,2} > \eta_{E,3} > \eta_{E,4}$ at all turbulence intensities (Fig. 2a), reflecting that smaller drops with weaker gravitational differential settling and higher ξ receive proportionally larger turbulent enhancement. This qualitative ordering matches the hierarchical signature of turbulent collision enhancement reported by Wang et al. (2005) and Chen et al. (2018) from direct numerical simulation of particle-laden turbulence, reproducing the physically expected behaviour that gravitationally efficient large drops benefit little from turbulent enhancement while gravitationally subdominant small drops benefit substantially.

7.5 Falsifiable predictions and the validation programme ahead

The three established validations of Section 7.4 are sufficient to anchor the unified framework against the asymptotic and qualitative published record. The framework also generates

https://doi.org/10.5194/egusphere-2026-2627
Preprint. Discussion started: 1 July 2026

three further specific quantitative predictions that map onto particular DNS or observational measurements but lie outside the scope of the present paper, which is concerned with deriving the unified kernel and demonstrating its asymptotic-limit consistency. We catalogue these predictions here as the explicit follow-up validation programme of the framework. Each requires the dedicated extraction or fitting of specific quantities from published datasets that are not available in standardised tabulated form, and is therefore deferred to dedicated follow-up studies beyond the present derivation paper.

Prediction 1: velocity boost $(1+\xi)$ versus Ayala et al. (2008). The effective approach velocity $|\Delta v_t^{\text{eff}}| = A_k(1+\xi)$ enhances the geometric collision rate independently of the collision efficiency. This is directly testable against the DNS study of Ayala et al. (2008), whose Part 1 paper focuses specifically on the geometric collision rate of sedimenting droplets in homogeneous turbulence, deliberately excluding efficiency effects in order to isolate the kinematic contribution. They report the radial relative velocity and pair-correlation function of drop pairs as a function of separation. Our prediction $(1+\xi) = 1.72$ at $N_k = 3$ and $\varepsilon = 10^{-3}\,\mathrm{m^2 s^{-3}}$, evaluated at the mean inter-drop separation $\bar{s}$, sets a specific quantitative target for the turbulent enhancement of the radial relative velocity. Point-by-point comparison requires extraction of the relative-velocity profile $|\Delta v|(s)$ at the specific separation $\bar{s}$ from their published dataset, and will be pursued in a dedicated follow-up study.

Prediction 2: efficiency enhancement η_E versus Chen et al. (2018). The closed-form prediction $\eta_E(\mathrm{Stk}, \xi)$ shown in Figs. 1(c) and 2(a) is directly testable against the DNS study of Chen et al. (2018), who isolate the turbulent modification of collision efficiency from purely kinematic effects. Their simulations report dimensionless efficiency-enhancement factors for cloud-droplet pairs at typical cumulus dissipation rates, with the same physical definition as our η_E. Our predicted range $\eta_E \in [1.00, 10.23]$ across the three size-gap hierarchical levels at $\varepsilon = 10^{-3}\,\mathrm{m^2 s^{-3}}$ provides a specific functional form $\eta_E(\mathrm{Stk}, \xi)$ against which individual DNS data points can be benchmarked. A systematic point-by-point benchmark against their reported efficiency values across the relevant Stokes-number range will form the second component of the planned follow-up validation study.

Prediction 3: DSD tail exponent versus CAMP^{2}Ex observations. The kernel exponent $4 - \alpha_3^{\text{eff}} = 2.361$ at the $N_k = 3$ level lies intermediate between the gravity-only exponent 2.500 and the turbulence-only exponent 2.167, and propagates into the power-law tail of the cloud-base drop size distribution via the Smoluchowski integral. Chandrakar et al. (2024) show from coupled large-eddy simulations and CAMP^{2}Ex observational data that the observed DSD tail near cloud base follows a power-law scaling that cannot be reproduced by either purely gravitational or purely turbulent kernels, implying an intermediate exponent consistent with our prediction. Quantitative fitting of the observed DSD power-law slope at $R \approx 15$ to $20\,\mu$m from CAMP^{2}Ex in-situ probe data, together with

https://doi.org/10.5194/egusphere-2026-2627
Preprint. Discussion started: 1 July 2026

forward evolution of the unified kernel through the Smoluchowski integral to predict the cloud-base DSD shape, will form the third and most observationally demanding component of the planned follow-up programme.

Because the unified framework contains no free parameters, each of the three predictions is a genuine falsification target rather than a calibration exercise. The validation programme as a whole is structured to test each of the framework's two orthogonal turbulent corrections separately before testing their combined observational consequence: passing Predictions 1 and 2 individually is a stricter test than passing a single-multiplier empirical enhancement factor, because the framework requires the two factors $(1 + \xi)$ and η_E to agree separately with independent DNS datasets while also multiplying to match the combined enhancement of Wang et al. (2005), whose foundational DNS study provides an auxiliary consistency check on the combined factor $(1 + \xi)\eta_E$. We view the present paper as completing the framework-derivation and asymptotic-limit-validation phase, with the quantitative DNS and observational comparisons constituting the natural next phase of the programme.

7.6 Limitations and extensions

Several important effects lie outside the present treatment. The terminal-velocity limit ($\tau_{\mathrm{St}} \to 0$) excludes finite-Stokes-number effects that alter the effective α_k^{eff} for drops with $\mathrm{St}_k \sim \mathcal{O}(1)$. The near-field hydrodynamic term (s^{-2}) has been subsumed into the Pinsky (2001) tabulated collision efficiency rather than derived within the fractional framework. A first-principles derivation of E_{Pinsky} from the hierarchical framework is a natural direction for future work. The framework applies to hierarchical configurations satisfying $R_k \gg R_{k-1}$. Collisions between drops of similar size require a separate treatment. Condensation, supersaturation fluctuations, and entrainment-mixing modify the DSD between collision events and are not captured by the purely dynamical framework. Preferential concentration effects, which enhance pair statistics in turbulent flows beyond the mean-field approximation used here, are known to contribute to η_E at intermediate Stokes numbers and will modify the predicted enhancement. Extension to ice-phase microphysics and the Bergeron-Findeisen process is a natural direction for future work.

8 Conclusions

We have derived and validated a unified closed-form collision kernel for warm-cloud coalescence that interpolates continuously between the laminar and turbulent asymptotic regimes through the dimensionless turbulence-to-gravity ratio ξ, and we have shown that three classes of established results in the literature are recovered as validations of the framework rather than as predictions awaiting test. The main results are as follows.

Earth's gravity plays two distinct roles. It acts as a body force that cancels from

https://doi.org/10.5194/egusphere-2026-2627
Preprint. Discussion started: 1 July 2026

relative-coordinate dynamics, and as the source of size-dependent differential settling velocities $K_{\mathrm{St}}R^2$ that drive inter-level collisions. Turbulence contributes an additional $s^{1/3}$ Kolmogorov-scaling relative velocity, with the gravity-turbulence crossover occurring at $s^* = [K_{\mathrm{St}}(R_k^2 - R_{k-1}^2)/C_0\varepsilon^{1/3}]^3$. A single dimensionless parameter, the turbulence-to-gravity ratio $\xi = B\bar{s}^{1/3}/A_k$, controls every aspect of the unified description.

The effective fractional parameter α_k^{eff} (Theorem 1) reduces to the gravitational scaling law $\alpha_k = 2 - 2/(N_k+1)$ of Chishtie (2026) when turbulence vanishes, and rises continuously toward $7/3 - 2/(N_k+1)$ as turbulence intensifies. Under warm-cloud reference conditions, the computed values are $\alpha_2^{\mathrm{eff}} = 1.580$, $\alpha_3^{\mathrm{eff}} = 1.639$, and $\alpha_4^{\mathrm{eff}} = 1.651$. The crossover scale s^* passes through the mean inter-drop separation $\bar{s}$ precisely at the $N_k = 3$ level ($s^*/\bar{s} = 2.73$, $R_k = 10 \to 20\,\mu$m, $\xi = 0.716$), providing a dynamical definition of the rain-initiation bottleneck as the hierarchical level at which $\xi(\bar{s}) \approx 1$.

Parametric solutions $s_k(\theta) = s_0 \sin^n\theta$ with $n = 2/(p_k^{\mathrm{eff}} + 1)$ are validated against RK45 integration to relative errors of $\sim 10^{-13}$, confirming machine-precision accuracy of the closed-form solution (14).

The unified collision kernel

$$K = \pi(R_k + R_{k-1})^2 \cdot A_k(1+\xi) \cdot E_{\mathrm{Pinsky}}(R_k, R_{k-1}) \cdot \eta_E(\mathrm{Stk}, \xi)$$

is validated against three independent established results: it reduces exactly to Hall (1980) and Pinsky et al. (2001) in the laminar limit $\varepsilon \to 0$, reproduces the characteristic Kolmogorov $\varepsilon^{1/3}$ scaling of Saffman–Turner (1956) in the high-ε limit, and matches the qualitative hierarchical ordering of turbulent collision enhancement reported by Wang et al. (2005) and Chen et al. (2018) from DNS. Away from the asymptotic limits, the framework introduces two independently testable turbulent corrections, a velocity boost $(1+\xi)$ and an efficiency enhancement η_E, both derived in closed form without free parameters. At the rain-initiation bottleneck ($N_k = 3$, $R_{k-1} = 10\,\mu$m $\to R_k = 20\,\mu$m, $\varepsilon = 10^{-3}\,\mathrm{m^2 s^{-3}}$), the framework predicts a collision kernel exceeding the Hall (1980) reference by a factor of 2.17, decomposed as a 1.72× velocity boost and a 1.26× efficiency boost. The framework achieves $\mathcal{O}(N \log N)$ computational complexity versus $\mathcal{O}(N^2)$ for existing super-droplet methods and is directly implementable in bin microphysics and LES super-droplet schemes. The three quantitative comparisons catalogued in Section 7, against the DNS studies of Ayala et al. (2008) and Chen et al. (2018) and the CAMP^{2}Ex observational analysis of Chandrakar et al. (2024), constitute the natural follow-up validation programme of the framework, which we intend to pursue next.

https://doi.org/10.5194/egusphere-2026-2627
Preprint. Discussion started: 1 July 2026

Code and data availability

All Python code used to produce the figures and tables is available at https://colab.research.google.com/drive/1S8EgXOQk8qdC3KXoadipiMh8Aw3AeHC7?usp=sharing. This is a self-contained Google Colab notebook that reproduces all results in this paper upon execution, including the unified collision kernel of Section 5 and Figs. 1 to 3.

Acknowledgements

The author thanks Prof. Roland B. Stull and Prof. Philip Austin (University of British Columbia) for discussions on cloud microphysics and fractional dynamics, and acknowledges the Peaceful Society, Science and Innovation Foundation (Vancouver) for supporting this research. The author is grateful to the anonymous reviewer of an earlier version of this manuscript, whose observation that the original framework did not explicitly carry a collision efficiency motivated the development of the unified kernel of Section 5.

Author contributions

F.A.C. conceived the study, developed the analytical framework and related methodology, wrote the code, and drafted the manuscript.

Competing interests

The author declares no competing interests.

References

Ayala, O., Rosa, B., Wang, L.-P., and Grabowski, W. W.: Effects of turbulence on the geometric collision rate of sedimenting droplets. Part 1. Results from direct numerical simulation, *New J. Phys.*, 10, 075015, 10.1088/1367-2630/10/7/075015, 2008.

Berry, E. X.: Cloud droplet growth by collection, *J. Atmos. Sci.*, 24, 688–701, 10.1175/1520-0469(1967)024<0688:CDGBC>2.0.CO;2, 1967.

Bott, A.: A flux method for the numerical solution of the stochastic collection equation, *J. Atmos. Sci.*, 55, 2284–2293, 10.1175/1520-0469(1998)055<2284:AFMFTN>2.0.CO;2, 1998.

Chandrakar, K. K., Morrison, H., Grabowski, W. W., and Lawson, R. P.: Are turbulence effects on droplet collision–coalescence a key to understanding observed rain formation

https://doi.org/10.5194/egusphere-2026-2627
Preprint. Discussion started: 1 July 2026

in clouds?, *Proc. Natl. Acad. Sci. USA*, 121, e2319664121, 10.1073/pnas.2319664121, 2024.

Chen, S., Yau, M. K., and Bartello, P.: Turbulence effects of collision efficiency and broadening of droplet size distribution in cumulus clouds, *J. Atmos. Sci.*, 75, 203–217, 10.1175/JAS-D-17-0123.1, 2018.

Chishtie, F. A.: Exact closed-form solutions to hierarchical many-body problems via fractional dynamics and elementary function representations, *Physics Open*, 27, 100391, 10.1016/j.physo.2026.100391, 2026.

Devenish, B. J., Bartello, P., Brenguier, J.-L., Collins, L. R., Grabowski, W. W., IJzermans, R. H. A., Malinowski, S. P., Reeks, M. W., Vassilicos, J. C., Wang, L.-P., and Warhaft, Z.: Droplet growth in warm turbulent clouds, *Q. J. R. Meteorol. Soc.*, 138, 1401–1429, 10.1002/qj.1897, 2012.

Grabowski, W. W. and Wang, L.-P.: Growth of cloud droplets in a turbulent environment, *Annu. Rev. Fluid Mech.*, 45, 293–324, 10.1146/annurev-fluid-011212-140750, 2013.

Hall, W. D.: A detailed microphysical model within a two-dimensional dynamic framework: model description and preliminary results, *J. Atmos. Sci.*, 37, 2486–2507, 10.1175/1520-0469(1980)037<2486:ADMMWA>2.0.CO;2, 1980.

Hoffmann, F., Dziekan, P., and Pawlowska, H.: The critical number and size of precipitation embryos to accelerate warm rain initiation, *Atmos. Chem. Phys.*, 25, 5313–5330, 10.5194/acp-25-5313-2025, 2025.

Khain, A. P., Beheng, K. D., Heymsfield, A., Korolev, A., Krichak, S. O., Levin, Z., Pinsky, M., Phillips, V., Prabhakaran, T., Teller, A., van den Heever, S. C., and Yano, J.-I.: Representation of microphysical processes in cloud-resolving models: spectral (bin) microphysics versus bulk parameterization, *Rev. Geophys.*, 53, 247–322, 10.1002/2014RG000468, 2015.

Koch, D. L., Dhanasekaran, J., Roy, A., and Sundaram, S.: The effect of turbulence, gravity, and non-continuum hydrodynamic interactions on the drop size distribution in clouds, *J. Atmos. Sci.*, in press, preprint: arXiv:2501.01086, 2025.

Pinsky, M., Khain, A., and Shapiro, M.: Collision efficiency of drops in a wide range of Reynolds numbers: effects of pressure on spectrum evolution, *J. Atmos. Sci.*, 58, 742–764, 10.1175/1520-0469(2001)058<0742:CEODIA>2.0.CO;2, 2001.

Pruppacher, H. R. and Klett, J. D.: *Microphysics of Clouds and Precipitation*, 2nd edn., Kluwer Academic, Dordrecht, 1997.

https://doi.org/10.5194/egusphere-2026-2627
Preprint. Discussion started: 1 July 2026

730 Saffman, P. G. and Turner, J. S.: On the collision of drops in turbulent clouds, *J. Fluid*
731 *Mech.*, 1, 16–30, 10.1017/S0022112056000020, 1956.

732 Shaw, R. A.: Particle–turbulence interactions in atmospheric clouds, *Annu. Rev. Fluid*
733 *Mech.*, 35, 183–227, 10.1146/annurev.fluid.35.101101.161125, 2003.

734 Shima, S., Kusano, K., Kawano, A., Sugiyama, T., and Kawahara, S.: The super-droplet
735 method for the numerical simulation of clouds and precipitation: a particle-based
736 and probabilistic microphysics model coupled with a non-hydrostatic model, *Q. J. R.*
737 *Meteorol. Soc.*, 135, 1307–1320, 10.1002/qj.441, 2009.

738 Wang, L.-P. and Grabowski, W. W.: The role of air turbulence in warm rain initiation,
739 *Atmos. Sci. Lett.*, 10, 1–8, 10.1002/asl.210, 2009.

740 Wang, L.-P., Franklin, C. N., Krueger, S. K., and Gibbs, J. A.: Turbulent enhancement of
741 collision rates of cloud droplets, *New J. Phys.*, 7, 27, 10.1088/1367-2630/7/1/027, 2005.

742 Zmijewski, P., Dziekan, P., and Pawlowska, H.: Modeling collision–coalescence in particle
743 microphysics: numerical convergence of mean and variance of precipitation in cloud
744 simulations using the University of Warsaw Lagrangian Cloud Model (UWLCM 2.1),
745 *Geosci. Model Dev.*, 17, 759–780, 10.5194/gmd-17-759-2024, 2024.